JOURNAL OF APPLIED ELECTROCHEMISTRY 19 (1989) 354–360

An experimental study of anodic dissolution of copper in aqueous sodium chloride via laser-induced image processing

Z. H. GU, T. Z. FAHIDY

Department of Chemical Engineering, University of Waterloo, Waterloo, Ontario, Canada N2L 3G1

Received 16 August 1988; revised 15 November 1988

The formation of a Cu_2O precipitate induced via anodic copper dissolution in an aqueous sodium chloride electrolyte was studied over the pH range 1–7 by means of laser illumination and digital processing of video images. A mechanism of precipitation is proposed on the basis of the experimental findings and the theory of ionic equilibria.

1. Introduction

The dissolution of metallic copper from an anode in aqueous $NaClO_3$ and NaCl solutions has attracted numerous researchers interested in its oscillatory behaviour [1], kinetics and mechanism [2–4] and corrosion properties [5–11]. It has been proposed that during the dissolution process an anodic film is formed temporarily and then dissolved according to the reaction steps [2–4]:

$$Cu + Cl^- \longrightarrow CuCl + e^- \quad (1)$$

$$CuCl + Cl^- \Leftrightarrow CuCl_2^- \quad (2)$$

The global dissolution rate increases with increasing chloride ion concentration; if the latter is sufficiently high, the formation of the $CuCl_3^{2-}$ complex is also important. Tribollet *et al.* [10, 11] propose that oxygen reduction on the cathode first results in a mixture of Cu_2O and CuCl deposited on the electrode which eventually (at immersion times larger than about an hour) is transformed fully into Cu_2O. While these studies throw light on the kinetic aspects and the mechanism of anodic copper dissolution and the nature of the dissolution products deposited on the electrodes, very little is known, apparently, about changes in flow structure in the electrolyte due to dissolution and the propagation of the precipitate in the electrolyte bulk: the authors are unaware of a systematic study of such aspects of the process. The purpose of this paper is to present an experimental study of these properties where a high-power laser source was used to illuminate the electrolyte solution in order to follow the formation and the motion of the precipitate obtained in the dissolution process. The laser technique is especially attractive on account of its particular sensitivity to phase-interface variations [12–14]. While in a previous investigation [14] of the technique feasibility the electrolyte pH was kept near 7.0, the current study embraces a much wider range ($1.0 \leqslant pH \leqslant 7.0$) in order to demonstrate that, although the speed of formation and the distribution of the precipitate is strongly pH dependent, Cu_2O precipitation can occur under appropriate conditions at a pH at least as low as 1.0. Quantitative measures of precipitate distribution which have been obtained by the development of a specific digital image-processing and analysis technique may well prove to be useful in a large variety of electrochemical processes where the motion of product precipitate could be followed and analysed in a similar manner.

2. Experimental details

The apparatus, shown in Fig. 1 consists of three components: electrochemical equipment, photographic equipment and computer hardware for image processing. Anodic dissolution was generated by current passed between pure copper electrodes in an electrolytic cell of cross-sectional area 35 mm × 25 mm, and 28 mm high. The electrodes were polished with fine-grain emery paper then washed and rinsed with deionized water and a small amount of acetone. The dried electrodes were placed into grooves separated at a distance of 34 mm. The electrolyte was prepared by dissolving analytical grade NaCl in deionized water and its pH was set carefully by adding aliquot amounts of HCl or NaOH solutions. Electrolysis was carried out by means of a Harrison 6203-B programmable regulated d.c power supply. A 2.5 W argon laser operating in continuous wave mode served as the illumination source: the beams was transformed into a thin (about 1 mm) light sheet via a glass rod/mirror assembly [15]. The exact position of the incident light sheet in the cell was controlled by a Mitutoyo digimatic caliper. Continuous recording of images was carried out by a video system and individual pictures (frames) were taken, where desired, by a photographic assembly whose detailed functioning has been described elsewhere [14–16].

The video data were transmitted directly into the memory bank of an IBM XT microcomputer by an OCULUS-200 image digitizer board; much of the required software for image processing is part of the

0021-891X/89 $03.00 + .12

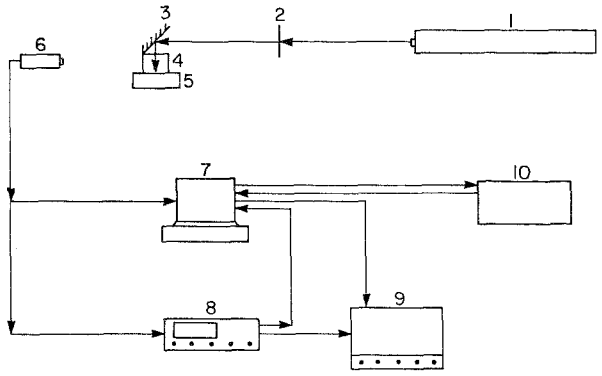

Fig. 1. Schematic of the overall experimental apparatus. 1, Laser source; 2, glass rod; 3, directing mirror; 4, electrolytic cell; 5, cell support; 6, video camera; 7, IBM XT microcomputer; 8, video recorder; 9 video monitor; 10, mainframe computer.

graphics package available on the University of Waterloo mainframe network, interconnected with the microcomputer via a SYTEK communication link. The major experimental parameters are assembled in Table 1.

In a preliminary set of experiments the chemical composition of the precipitate filtered from elecrolyte solutions was confirmed to be Cu_2O via a conventional X-ray diffraction test. In subsequent experiments the electrolyte pH was systematically lowered from 7.0 to 1.0 and the same electrolytic procedure was carried out using fresh electrodes and electrolyte solutions. It was found in general that precipitate growth rate and distribution are strongly pH dependent, but at all values of the experimental pH, Cu_2O is formed first at the vicinity of the cathode, reaching various portions of the electrolyte bulk upon subsequent propagation. The higher the pH the faster the formation of the precipitate and its propagation into the electrolyte. Figure 2 illustrates a typical history of precipitate formation at pH = 6; first appearance is detected at the upper cathodic region at about 2 min (Fig. 2a) after the onset of electrolysis denoted as zero time in all figures. Thus, all time instants in the sequel represent time lapsed past the onset of electrolysis.

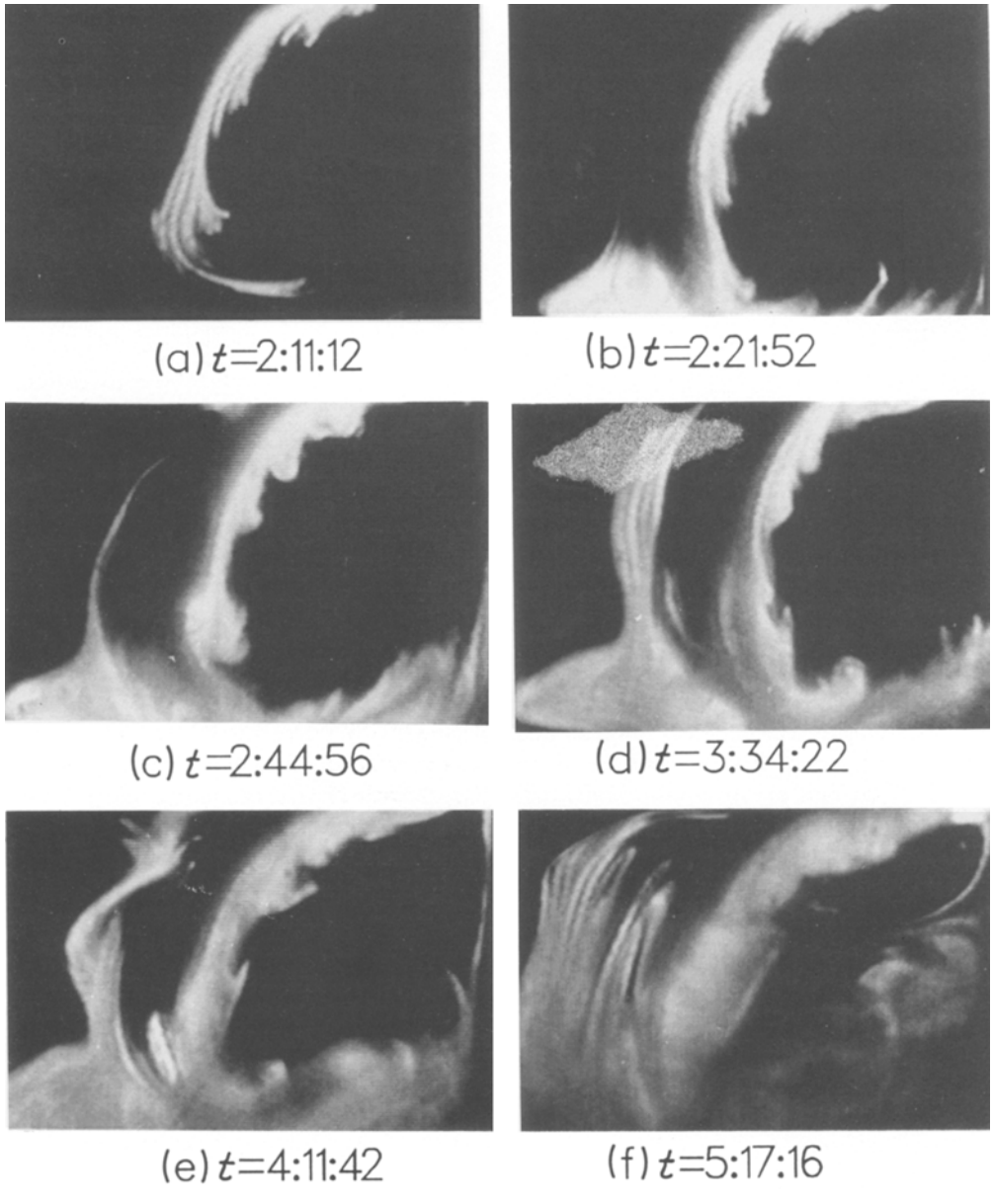

Fig. 2. Development of precipitation during electrolysis at pH 6.0. The cathode is located at the right and the time elapsed during electrolysis is indicated below the figure.

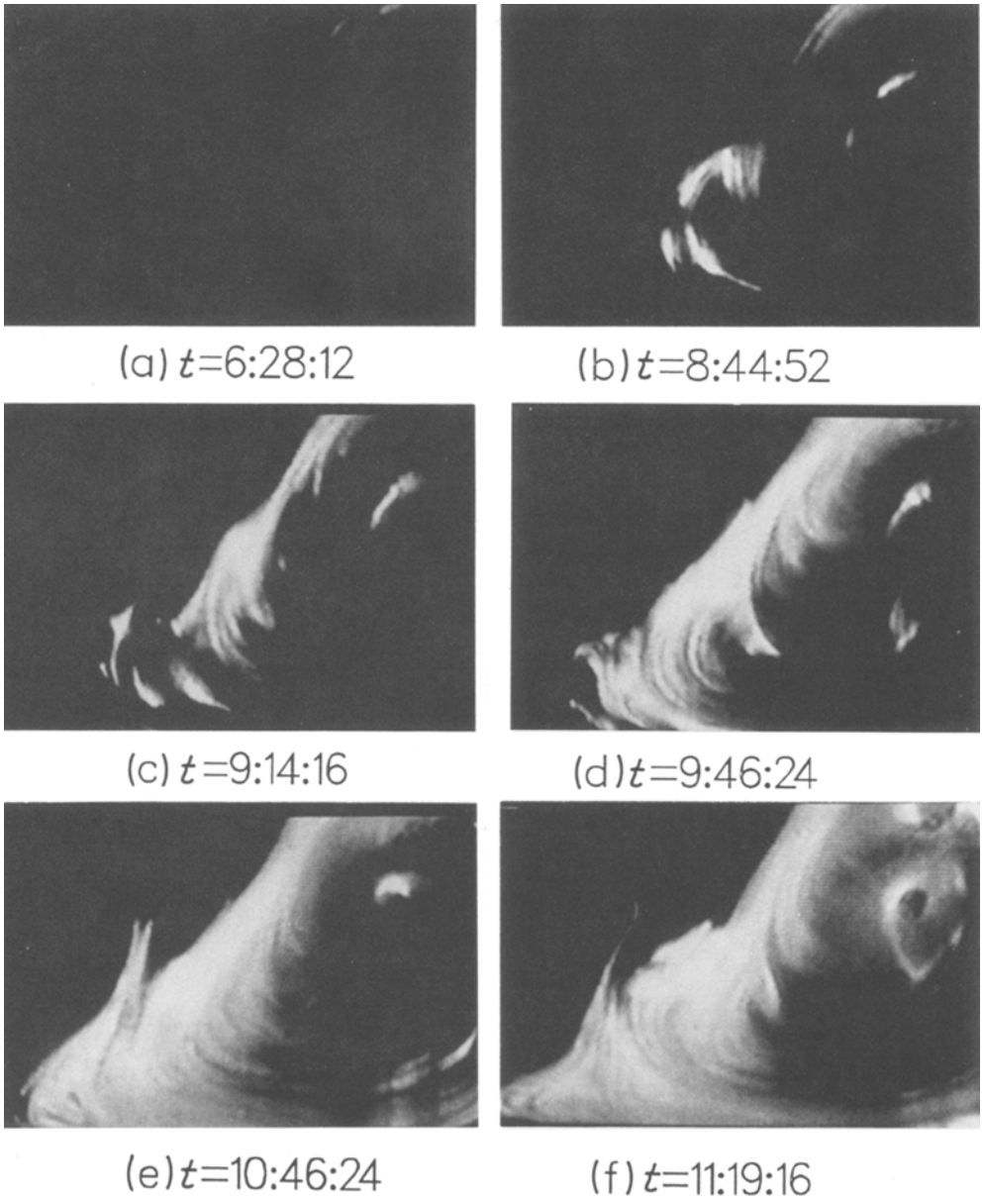

Fig. 3. Development of precipitation during electrolysis at pH 2.0.

Gradual penetration into the bulk solution is followed by recirculation towards the cathode (Fig. 2b). At about 3 min (Fig. 2c) the growth of the precipitate phase is sufficient for the leading edge to split into two 'branches' near the bottom. One expands towards the anode while the other branch rises towards the electrolyte surface (Figs 2d and e). By about 5 min the majority of the illuminated cross-section is occupied by precipitate but, as shown by the transparent sections, the upper region at the anode and the centre of circulation are essentially devoid of solid phase.

The appearance of precipitate is appreciably delayed with a decrease in pH, as indicated by Fig. 3, at otherwise identical experimental conditions. At pH 2.0 the electrolyte remains fully transparent for about 3 min after the onset of electrolysis, then a fine-structured precipitate persists until about 6.5 min (Fig. 3a). Growth is slow and circulation is not observed clearly until about 9 min (Fig. 3b); the precipitate is essentially confined to the cathodic region (Fig. 3c–e), its lower portion finally beginning to move towards the anode (Fig. 3d). The precipitate is dense and the boundary between the solid and liquid phase is very sharp.

Table 1. Summary of the experimental parameters

Parameter	*Unit*	*Magnitude*
pH		1.0–7.0
NaCl	$mol\,dm^{-3}$	1.504
D.c. voltage	V	1.5
Current density	$mA\,cm^{-2}$	12.56
Position of the illuminating laser sheet (from front cell wall)	mm	15.06

3. Digital processing and analysis of video data

Qualitative information obtained by photography (video or otherwise) is complemented by digitization

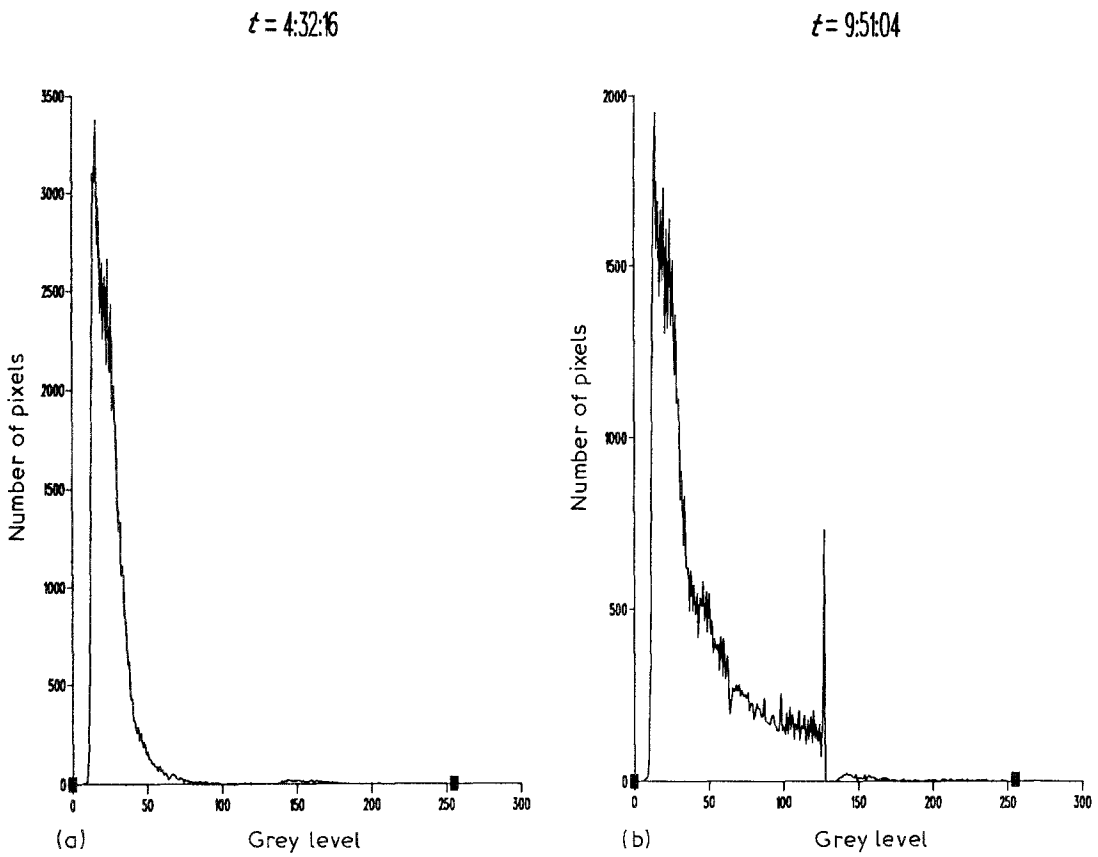

Fig. 4. Grey-level distribution (histogram) at a selected time instant, at pH 2.0. (a) t = 4 min 32.16 s; (b) t = 9 min 51.4 s.

of images which yields a quantitative description of precipitate formation and movement. Recorded video data were converted into digital images using an OCULUS-200 digitizer board with 480 × 512 pixel resolution, generating a 0–255 grey level range (the pixel is the smallest element of a digital image and the light intensity of the image at a given location is represented by the grey level). When the electrolyte is illuminated before electrolysis, it is uniformly transparent and the corresponding light intensity serves as the zero (or reference) grey level, $G = 0$. As precipitation commences and the number of precipitate particles increase, the number of pixels N and the value of G increase correspondingly, providing an easily monitored measure of the precipitation process. Figure 4 is a typical frequency distribution diagram of grey levels indicating the degree of precipitate formation at pH = 2. Figure 4a shows an early stage (at about 4.5 min) where most of the pixels are at a low grey level (N_{max} = 3374 at G = 16); there is little precipitation up to this time. The second peak (N = 732 at G = 127) appearing in Fig. 4b indicates that a considerable amount of precipitate was formed during the next minute of electrolysis.

Image analysis can also be used to compute at any given time and at an arbitrary grey level, the area occupied by precipitate particles at an illuminated section of the electrolytic cell. Figure 5 is a typical area–kinetic plot at G = 80 which can be considered as a threshold grey level, G_t, in the sense that $G < G_t$ represents a negligible amount of precipitation, in the experimental apparatus. Then, the relative rate of precipitate accumulation (due to local formation and propagation from other sections of the cell) may be described via A versus time curves where

$$A \equiv \frac{\text{portion of the illuminated section where } G \geqslant G_t}{\text{total area of the illuminated section}} \times 100\% \quad (3)$$

Figure 6 portrays typical accumulation curves at two different pH values at the illuminated section, which are characterized via three different zones. The first portion, observed at small times, is the zone of slow growth where the amount of precipitate is very small. In the next zone A increases sharply and near-linearly with time; in the third zone precipitate accumulation slows considerably and its growth with time remains modest throughout the remainder of the process. The three-zone property of accumulation kinetics is also indicated by the rate of change defined at each observation instant t_i as:

$$S_i \equiv \frac{A_{i+1} - A_i}{t_{i+1} - t_i}; \quad i = 1, 2, \ldots \quad (4)$$

As shown in Table 2, the existence of the three zones is pH independent, but the zones appear at increasingly earlier times as the pH is increased. It is instructive to consider the time of attainment for A = 20, which is the approximate position of the inflection point on the A/t curves, given in Table 3. The regressions

$$\log_{10} t_{20} = 2.9877 - 0.12257\,\text{pH}, \quad r^2 = 0.989 \quad (5)$$

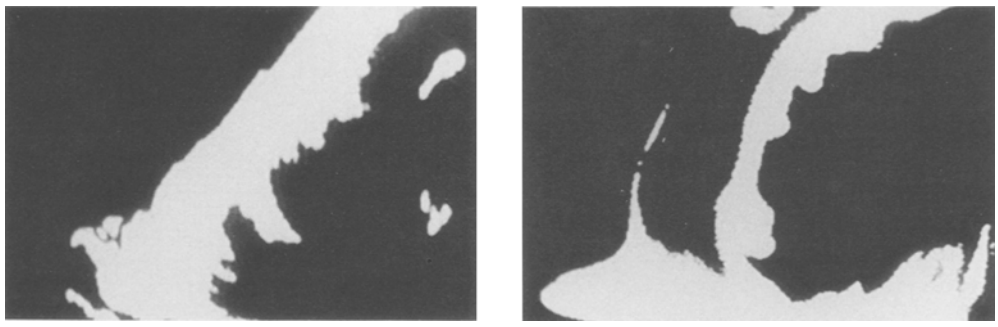

Fig. 5. Precipitate distribution at a grey level of 80.

and

$$t_{20} = 746.857 - 95.0714\,\mathrm{pH}$$
$$r^2 = 0.962 \quad (6)$$

indicate a high degree of linear association between pH, t_{20} and log t_{20} but it is not known at present if this result has a particular physical significance (r^2 is the coefficient determination in the regression analysis). The quantitative demonstration of the delaying effect of acidity on precipitate accumulation is, in any event, a cornerstone result for the mechanism of Cu_2O formation proposed in the next section.

4. The mechanism of precipitate formation and propagation

As discussed by Butler [17] the reaction steps involving cuprous ions and chloride ions have the following equilibrium constants at 25° C:

(1) $Cu^+ + Cl^- \longrightarrow CuCl$

$$K_1 = [Cu^+][Cl^-] = 1.86 \times 10^{-7} \quad (7)$$

(2) $CuCl + Cl^- \longrightarrow CuCl_2^-$

$$K_2 = [CuCl_2^-]/[Cl^-] = 0.0758 \quad (8)$$

(3) $CuCl_2^- + Cl^- \longrightarrow CuCl_3^{2-}$

$$K_3 = [CuCl_3^{2-}]/[Cl^-]^2 = 0.0339 \quad (9)$$

The Cu^+ ions are supplied by anodic dissolution according to the electrochemical reaction

(4) $Cu \longrightarrow Cu^+ + e^- \quad E_o = -0.521\,V \quad (10)$

The cathode process consists of proton discharge, and the reduction of oxygen:

(5) $O_2 + 2H_2O + 4e^- \longrightarrow 4OH^-$

$$E_o = 0.401\,V \quad (11)$$

In the presence of OH^- ions the dichloride complex undergoes a further reaction producing the precipitate:

(6) $2CuCl_2^- + OH^-$

$$\longrightarrow Cu_2O(s) + H^+ + 4Cl^- \quad (12)$$

The overall free energy change in Reaction 6 is computed from standard free energy data [18] as $\Delta G^0 = -33.444\,\mathrm{kJ\,mol^{-1}}$, hence $K_6 = 7.28 \times 10^5$ at 25° C. The chloride ion concentration at equilibrium may be obtained from the chlorine balance

$$M = [Cl^-] + 2[CuCl_2^-] + 3[CuCl_3^{2-}] \quad (13)$$

where M is the initial NaCl concentration in the solution, by direct substitution of Equations 8 and 9. The final explicit expression for chloride ion concentration is obtained as

$$[Cl^-] = \{[(2K_2 + 1)^2 + 12K_3M]^{1/2} - (2K_2 + 1)\}/6K_3 \quad (14)$$

It then follows that the minimum pH for precipitation

Table 2. The effect of pH on the relative rate of accumulation of the precipitate

Observation time index i	$t_i(s)$		A_i		$10^3 S_i(s^{-1})$		$10^3(S_i - S_{i-1})(s^{-1})$	
	pH 2	*pH 6*	*pH 2*	*pH 6*	*pH 2*	*pH 6*	*pH 2*	*pH 6*
1	349	68	0.4983	0.7534	2.330	0.194	2.330	0.194
2	457	102	0.7499	0.7600	11.63	2.210	9.302	2.016
3	482	112	1.0470	0.7821	50.78	2.833	39.05	0.623
4	532	124	3.5749	0.8121	217.5	332.5	166.9	329.7
5	554	147	8.3615	8.4650	309.9	493.0	92.37	160.4
6	591	172	19.8390	20.7900	327.2	236.3	17.31	−256.7
7	620	196	29.3198	26.4601	22.45	64.58	−304.8	−171.6
8	678	220	30.6441	28.0100	43.07	62.50	20.62	−2.083
9	711	244	32.0222	29.5102	20.36	20.34	−22.71	−42.13
10	722	271	32.2461	30.0601	–	–	–	–

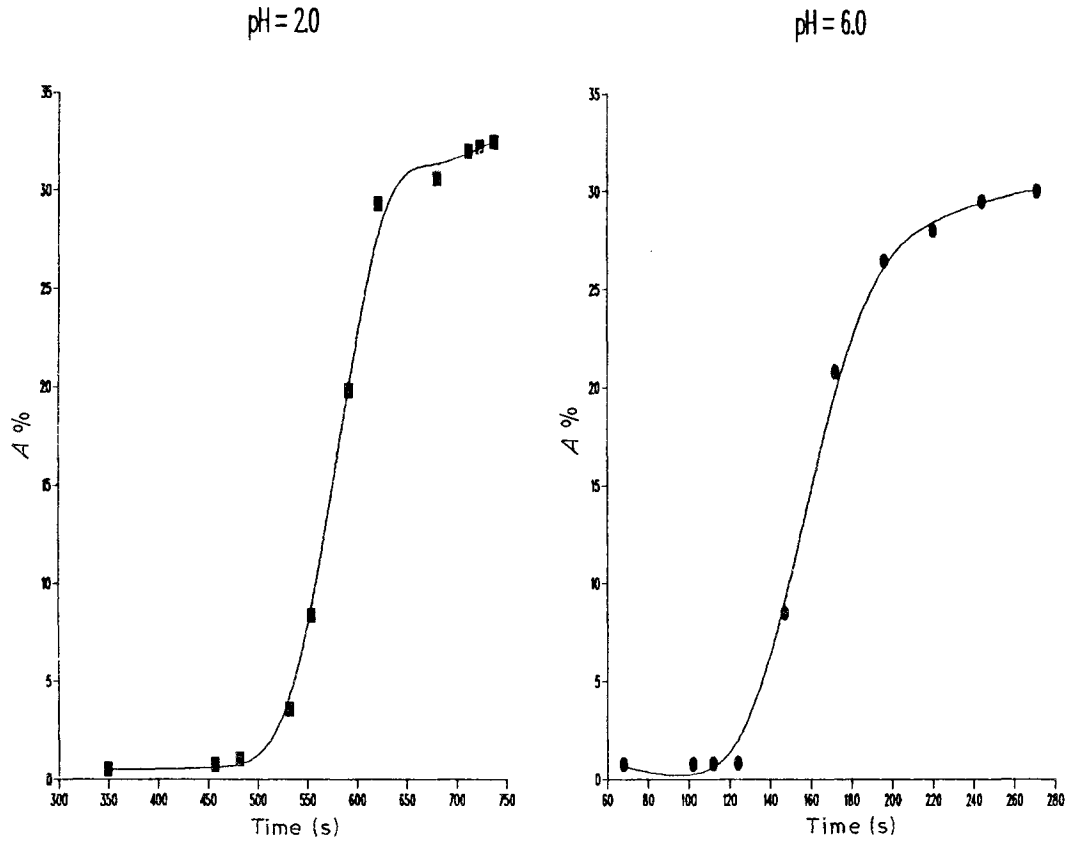

Fig. 6. Development of precipitation at pH 2.0 and 6.0.

may be computed from the relationship

$$pH = \log_{10}(1/K_2) + \tfrac{1}{2}\log_{10}(1/K_6K_w) + \log_{10}[Cl^-] \quad (15)$$

$$= 5.189 + \log[Cl^-] \quad (16)$$

since $K_w = [H^+][OH^-] = 10^{-14}$ at 25° C. As shown in Table 4, pH_{min} increases modestly with the initial salt concentration: in the current experiments with $M = 1.5\,mol\,dm^{-3}$ kept constant, no precipitation would be expected under equilibrium conditions below pH 5.26.

The reason for precipitate formation observed at much lower values of pH is supplied by the visualization experiments described above: cuprous complex ions travel across the cell from the anodic region to the cathodic region where the local pH is sufficiently higher (i.e. $pH \geqslant pH_{min}$) due to Process 5 (Equation 11) to induce precipitate formation in the vicinity of the cathode. Due to the gradual expansion of the region of relatively high local pH towards the bulk as electrolysis continues, and because of convection from the cathodic region into the bulk, the Cu_2O precipitate gradually penetrates the electrolyte solution. The induction time for precipitate formation and its penetration into the bulk increases with a decrease in the initial solution pH_0 since a larger ($pH_{min} - pH_0$) resistance to precipitate formation has to be overcome. The 'levelling out' tendency at relatively large times, shown in Fig. 6, is probably due to the balancing effect between the rate of precipitation arrival in a given section and the rate of precipitate dissolution in the lower pH environment, but there is yet no experimental information (over a sufficiently long time period) to ascertain whether a steady precipitate level is reached, or if there exists a demonstrably large hysteresis in dissolution.

The role of cupric ions in the overall process has not been investigated but theoretical considerations indi-

Table 3. The effect of pH on the time of attainment of the approximate inflection point (A = 20)

pH	t_{20} *(s)*
1.0	675
2.0	598
3.0	420
4.0	340
5.0	225
6.0	170
7.0	138

Table 4. The effect of NaCl concentration on the minimum pH required for Cu_2O precipitation

M ($mol\,dm^{-3}$)	$[Cl^-]$ ($mol\,dm^{-3}$) *(Equation 14)*	pH_{min} *(Equation 16)*
0.1	0.0862	4.12
0.5	0.4187	4.81
1.0	0.8103	5.10
1.2	0.9605	5.17
1.5	1.1796	5.26
2.0	1.5299	5.37

cate that it is negligible. The standard electrode potential is lower ($E_o = -0.33$ V) for the $Cu \rightarrow Cu^{2+} + 2e^-$ process than for the $Cu \rightarrow Cu^+ + e^-$ process and the $Cu^+ \rightarrow Cu^{2+} + e^-$ potential is much lower ($E_o = -0.153$ V). However, due to the formation of the cuprous complexes at an appreciable quantity (from Equation 14 and Equation 8, $[CuCl_2^-] = 0.089\,mol\,dm^{-3}$, from Equation 14 and Equation 9, $[CuCl_3^{2-}] = 0.047\,mol\,dm^{-3}$ at equilibrium, under the current experimental conditions) and since $[Cu^+] \cong 1.6 \times 10^{-7}\,mol\,dm^{-3}$ at equilibrium (from Equations 14 and 7), it is reasonable to assume that cupric ions exist only for a very short time in the solution.

5. Concluding remarks

The foregoing results demonstrate the capabilities of the laser-based visualization technique coupled with image digitization to assist studies of electrochemical process mechanisms by closely monitoring flow patterns and propagation structure in a multiphase electrolyte. Based on this study, a systematic investigation of the copper dissolution phenomenon under the influence of various process parameters has been initiated and its findings will be reported in future communications.

Acknowlegement

This project has been supported by the Natural Sciences and Engineering Research Council of Canada.

References

[1] J. F. Cooper, R. H. Muller and C. W. Tobias, *J. Electrochem. Soc.* **127** (1980) 1733.
[2] M. Braun and K. Nobe, *ibid* **126** (1979) 1667.
[3] H. P. Lee and K. Nobe, *Ibid* **132** (1985) 1037.
[4] *Idem, ibid.* **133** (1986) 2035.
[5] B. Miller, *ibid.* **116** (1969) 1117.
[6] B. Miller and M. I. Bellavance, *Ibid.* **119** (1972) 1510.
[7] W. H. Smyrl, in 'Comprehensive Treatise of Electrochemistry' (edited by J. O'M. Bockris, B. E. Conway, E. Yeager and R. E. White), Plenum, New York (1981) Vol. 4, p. 97.
[8] W. D. Bjorndahl and K. Nobe, *Corrosion* **40** (1984) 82.
[9] H. P. Dhar, R. E. White, G. Burnell, L. R. Cornwell, R. B. Griffin and R. Darby, *ibid.* **41** (1985) 317.
[10] C. Deslouis, G. Mengoli, M. M. Musiani and B. Tribollet, *J. Appl. Electrochem.* **18** (1988) 374.
[11] *idem, ibid* **18** (1988) 384.
[12] H. Imamoto and T. Ishigaki, in 'Visualization of Longitudinal Eddies in an Open Channel Flow, Flow Visualization IV' (edited by C. Véret), Hemisphere, Washington (1987) p. 333.
[13] E. L. Hanzevack, C. B. Bowers Jr and C. H. Ju, *AIChE J.* **33** (1987) 2003.
[14] Z. H. Gu and T. Z. Fahidy, *Int. J. Eng. Fluid Mech.* **1** (1988) 1.
[15] *Idem, J. Electrochem. Soc.* **134** (1987) 2241.
[16] *Idem,* 'A Video-Image Study of Electrolytic Flow Structure in Parallel Electric-Magnetic Fields, Flow Visualization IV' (edited by C. Véret), Hemisphere, Washington (1987) p. 333.
[17] J. N. Butler, 'Ionic Equilibrium, A Mathematical Approach', Addison-Wesley, Reading MA (1964).
[18] 'Lange's Handbook of Chemistry', Section 9, Table 9-1 (edited by J. A. Dean), McGraw Hill, New York (1979).